Characterization of the Solvation and Transport of the Hydrated Proton in the Perfluorosulfonic Acid Membrane Nafion

Matt K. Petersen and Gregory A. Voth*

Department of Chemistry and Center for Biophysical Modeling and Simulation, University of Utah, 315 South 1400 East, Room 2020, Salt Lake City, Utah 84112-0850

Received: May 3, 2006; In Final Form: July 14, 2006

The solvation and transport properties of the sulfonate−hydronium ion pair have been studied in hydrated Nafion through molecular dynamics simulation. Explicit proton and charge delocalization of the excess proton transport, via the Grotthuss hopping mechanism, were treated using the self-consistent multistate empirical valence bond (SCI-MS-EVB) method. The nature of the sulfonate−hydronium ion pair was characterized through analysis of free-energy profiles. It was found that, in general, the excess proton is solvated between two water molecules of a Zundel moiety while in the contact ion pair position, but then it transitions to an Eigen-like configuration in the solvent-separated pair position. Furthermore, the positive charge associated with the excess proton passes between the contact and solvent-separated ion pair positions through the Grotthuss mechanism rather than simple vehicular diffusion. The total proton diffusion was decomposed into vehicular and Grotthuss components and were found to be of the same relative magnitude, but with a strong negative correlation resulting in a smaller overall diffusion. Correlated motions between the ion pair were examined through the distinct portion of the van Hove correlation function, and a characteristic time scale of ∼425 ps was observed. Additionally, the association of the hydrated proton with the hydrophobic polymer backbone suggests its amphiphile-like behavior (see *Acc. Chem. Res.* **2006**, *39*, 143; *Phys. Rev.* **1954**, *95*, 249; *J. Chem. Phys.* **2005**, *123*, 084309).

1. Introduction

As an integral component of fuel cells, the electrolyte often dictates critical parameters such as weight, catalyst, and operational temperature range. Of the disparate types of conventional fuel cells available, only polymer electrolyte membrane fuel cells (PEMFC) have achieved the weight and operational temperature that is convenient for use in common consumer products such as portable electronics. PEMFC are able to use readily available and renewable fuels such as hydrogen and methanol while producing little emissions relative to the internal combustion engine. Furthermore, the infrastructure for the transportation, storage, and delivery of a volatile liquid like methanol is already in place for the distribution of gasoline. It is these attributes that are driving the rapidly growing interest in PEMFC as environmentally friendly power sources and have poised PEMFC to be a promising energy delivery technology for this century.

For PEMFC to become a practical, commercially available alternative to current energy delivery means, research efforts have focused on eliminating those properties which limit the fuel cell efficiency. Catalytic and transport rates generally increase with temperature, and as a result, attempts[1,2] have been directed at synthesizing polymer electrolyte membranes (PEMs) that do not degrade at high temperatures. Poisoning[3] of the catalytic process by reactants crossing the PEM has also been addressed.[4] While the limitations of current PEM can perhaps be mitigated through resourceful engineering, ultimately these efficiency-limiting properties should be directly addressed through the development of new and novel materials. Toward this end, a fundamental understanding of the underlying physics of proton transport within the PEM is critical.

Current PEMFC technology incorporates, almost exclusively, the perfluorosulfonic acid polymer membrane as the electrolyte. Many such membranes have been commercially available, for example, Nafion (Dupont), Aciplex (Asahi Chemical), and Dow membrane (Dow Chemical). These membranes exhibit favorable chemical stability in the highly reducing surroundings of the PEMFC as well as good thermal and mechanical stability. Of these, Nafion has been most studied and is perhaps the archetypal membrane. Substantial experimental effort has been put forth to characterize the structure and mass transport properties of Nafion. Investigations have included scanning electrochemical microscopy,[5] nuclear magnetic resonance and X-ray scattering,[6] differential scanning calorimetry and IR spectroscopy,[7] and neutron scattering,[8] to name just a few. Unfortunately, the local microscopic structure of hydrated Nafion is still not completely understood, largely due to the inhomogeneous nature of the material. Likewise, experiment has not provided direct evidence to describe the mechanism of proton transport. In an effort to aid in the characterization of both the structure and mechanism of proton transport, statistical mechanical modeling,[9−11] ab initio molecular modeling,[11−15] and molecular dynamics (MD) simulation have been performed.[12,16−21]

While experiment has failed to conclusively elucidate the microscopic PEM structure, the general concept of microscopic phase organization proposed by Gierke and Hsu[22,23] is widely accepted. The morphology of these distinct hydrophilic and hydrophobic regions is of significant interest because the hydrophilic ionic clusters most certainly facilitate proton transport within the membrane. Understanding the character of these regions is particularly important, and computer simulation

* Corresponding author. E-mail: voth@chemistry.utah.edu.

10.1021/jp062719k CCC: $33.50
Published on Web 08/26/2006

has contributed significantly here. For example, Jang et al.[19] have performed MD simulations with varying monomeric sequences of ~1100 equivalent weight (EW) Nafion, from which there is compelling evidence that identifies the true sequence and characteristic dimensions. The Hsu and Gierke cluster network model seems to be an oversimplification for what has been shown through experiment[5−8] and simulation[17−20] to be significantly more complicated phase segregation. However, MD simulations remain in reasonable agreement with the overall scheme of hydrophobic/hydrophilic domain segregation of the model proposed by Hsu and Gierke, while displaying the anticipated tortuous morphology.

Likewise, MD has been somewhat successful in describing dynamical properties such as ion transport. Selective ionic conductance, i.e., preferential transport of cations, has been demonstrated through simulations performed by Elliot et al.[20] Additionally, the hydration-dependent diffusive behavior of simple monovalent cations has been well described.[17] However, proton diffusion is markedly different from these monovalent cations in that an excess proton in water may move either through simple "vehicular" diffusion or by shuttling through the hydrogen bond network via the Grotthuss mechanism[24−26] of bond formation and cleavage. (It should be noted that a more recent picture of the Grotthuss shuttling mechanism in bulk water involves a significantly more complicated rearrangement of the underlying water hydrogen bond network than suggested in earlier papers.[27]) Statistical mechanical models have accurately reproduced proton diffusion rates [9−11] but are generally lacking actual dynamical information. Empirical models that employ simple hydronium force fields, which do not allow for bond cleavage and Grotthuss shuttling, have been used in several studies.[12,19,20] More sophisticated force fields have also been employed for the solvated proton. For example, Spohr et al.[28] have simulated explicit proton transport in a simplified membrane modeled as an excluded volume and, more recently, Seeliger et al.[29] have used a more rigorous all-atom treatment, both by means of a simplified two-state empirical valence bond model. However, this two-state model lacks the ability to appropriately delocalize the excess charge across all solvating water molecules, for example, in a strongly solvated Eigen-like $H_9O_4^+$ configuration.[30] This approximation will favor the Zundel cation $H_5O_2^+$ and hence omit the essential physics from the contribution of the Eigen cation.

The exploration for new PEM candidates is a realistic goal of molecular modeling. However, the most meaningful results are likely to come from a thorough and accurate description of the underlying molecular scale phenomena. It is the goal of this paper to take another step in that direction. The present authors have recently shown[21] through a fully atomistic simulation of a Nafion hydrophilic domain that a multistate empirical valence bond (MS-EVB) treatment[30] of an excess proton in Nafion leads to significantly different solvation structures and dynamics than a simple empirical classical hydronium model. Building upon that study, the present paper describes the first simulation of multiple Grotthuss shuttling excess protons in a hydrophilic Nafion domain. It employs the recently developed self-consistent iterative multistate empirical valence bond (SCI-MS-EVB) method of Wang and Voth,[31] which allows for multiple excess protons to be efficiently treated within an MS-EVB simulation.

2. Simulation Details

The present simulations consisted of four ~1100 EW Nafion oligomers, each composed of 10 uniformly spaced pendant monomers, with a water loading of 15 H_2O/SO_3^-. The potential used for the polymer was that of Jang et al.,[19] while the water and excess protons portion of the potential was treated by the self-consistent iterative multistate empirical valence bond (SCI-MS-EVB) method.[31] These potentials were mixed using the Lorentz−Berthelot mixing rules, and the Ewald summation method was employed for all electrostatic interactions. Theory[11] and experiment[7] indicate that, even at very low hydration, the excess proton is completely dissociated from the sulfonic acid group. So, as in our previous study[21] of which the present work is a generalization, protonated sulfonate groups were not included in the model, i.e., all were considered to be fully dissociated.

All MD simulations were constructed as follows: A starting configuration was created from randomly placed water and polymer at 50% of the experimental density. From this configuration, a constant temperature equilibration using a single-state (classical hydronium) approximation to the SCI-MS-EVB hydronium ion potential was carried out for 500 ps at 400 K, followed by 1 ns of constant pressure/temperature equilibration at 1 atm and 300 K. Five configurations were then selected at evenly spaced intervals along a subsequent 200 ps constant volume/temperature trajectory at 300 K, with the final equilibrium density of 1.61 gm/cm^3. These configurations were then equilibrated with the full SCI-MS-EVB potential for 200 ps at a constant temperature of 300 K. Last, the final configurations from the previous trajectories were used to start five distinct 500 ps microcanonical (constant NVE) trajectories from which a total of 2.5 ns of data were collected for analysis.

It is not entirely clear whether the previous procedure results in satisfactory equilibration of the polymeric backbone. In fact, the time scale required to adequately sample the phase space of the polymeric backbone of Nafion is prohibitive. We therefore assume that the polymeric backbone serves as a support for the significantly more mobile sulfonate-terminated side chains and as confinement for the hydrophilic domain. However, it is noteworthy that the equilibration procedure described above does result in similar microscopic structure and density as in previous studies with similar[17] and identical[19,21] polymeric backbone force fields. That is, the hydrophobic polymeric backbone and aqueous hydrophilic groups are organized into obviously segregated structures with clearly defined water and polymer phases. The hydrophilic phase is composed of water and sulfonate groups uniformly dispersed along the hydrophilic/hydrophobic interface. At this level of hydration, the hydrophilic domain forms a continuous subphase across the periodic boundaries.

Therefore, while we are optimistic that the backbone structures are likely representative of the dominant configurations, no attempt has been made in this study to characterize the average or dynamical behavior of this portion of the polymer. Because the overall macroscopic proton conductance must be modeled with much larger length and time scales, this study is limited to the local proton environment and dynamics accordingly.

The first portion of the discussion below will describe the nature of the sulfonate−SCI-MS-EVB hydronium ion pair and associated solvation structure. The second portion will focus on the dynamics of proton transport, followed by a discussion of the correlated motion of the ion pair. Finally, evidence for an anisotropic amphiphile-like association of the hydronium cation and the hydrophobic polymer backbone is presented through analysis of full and restricted radial distribution functions.

3. Results and Discussion

3.1. Free Energy of the Sulfonate−SCI-MS-EVB Ion Pair. In the multistate empirical valence bond (MS-EVB) ap-

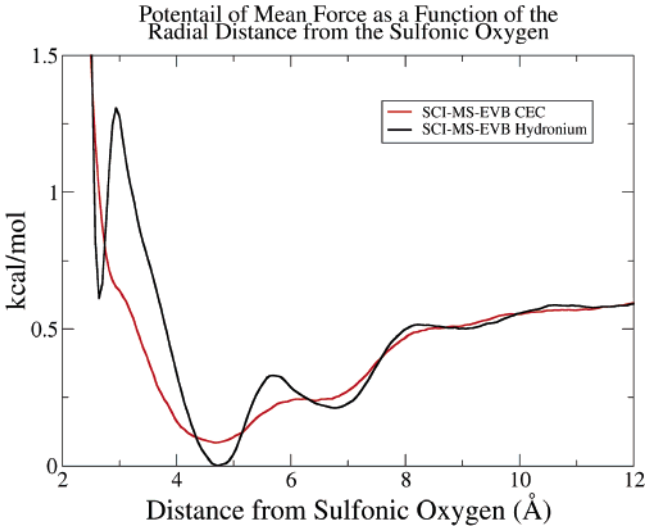

Figure 1. Potential of mean force (PMF) as a function of the radial distance between the sulfonate oxygen and hydronium oxygen (black curve) and the sulfonate oxygen and center of excess charge (CEC) (red curve).

proach[30,32,33] atomic coordinates are propagated over a ground-state potential energy surface constructed from the linear combination of coupled diabatic valence states. Typically, several EVB states contribute significantly, and consequently, identifying a single hydronium cation is not possible. One straightforward approach would be to use the dominant state from the linear combination of limiting states at a given time step. This description will hereafter be referred to as the hydronium description or simply the hydronium cation. Alternately, the coordinates of the charge defect associated with the excess proton can be used to describe the cation. This so-called center of excess charge (CEC) is defined[30] (eqs 1 and 2) as the center of excess charge for the hydronium cation from each contributing state i (CEC_i, eq 1), weighted by the EVB population of these states.

$$\overrightarrow{\mathrm{CEC}}_i = \left[\frac{\sum_{j}^{\mathrm{atoms}\,(\mathrm{H_3O^+})} |q|_{j;i}\, \vec{r}_{j;i}}{\sum_{j}^{\mathrm{atoms}\,(\mathrm{H_3O^+})} |q|_{j;i}} \right] \tag{1}$$

$$\vec{r}_{\mathrm{CEC}} = \sum_{i}^{\mathrm{states}} c_i^{\,2} (\overrightarrow{\mathrm{CEC}}_i) \tag{2}$$

Here, c_i^2 is the population of EVB state i, while $q_{j;i}$ and $\vec{r}_{j;i}$ are the charge and position of atom j of the hydronium cation in state i. Figure 1 illustrates the potential of mean force (PMF) along the radial distance from the sulfonate oxygen for the hydronium cation and CEC definitions.

The PMFs for each description are quite disparate; most notable is the absence of the barrier for the CEC PMF between the contact ion pair (CIP; configurations characterized by a hydrogen bond directly between the two ions) and the solvent-separated ion pair (SSIP; configurations characterized by an intervening solvent molecule to which both ions are directly hydrogen bonded, cf. Figure 2). The origin of this difference is the discrete nature of the hydronium description. There is a significant barrier for a single hydronium cation to transition between the CIP and SSIP region bearing the bulk of the excess charge. The CEC description displays no such barrier, as there is no need for any single molecule to overcome the hydronium CIP/SSIP barrier (i.e., the proton can shuttle between several water molecules). The CEC is therefore able to transition smoothly and in barrierless fashion through the hydrogen bonds of the adjacent water molecules occupying the CIP/SSIP positions. So clearly, the description of the hydronium as a single ion fails to capture some fundamental process in the transition of the cation between the CIP and SSIP regions, specifically because of the proton transport through the Grotthuss shuttling mechanism.

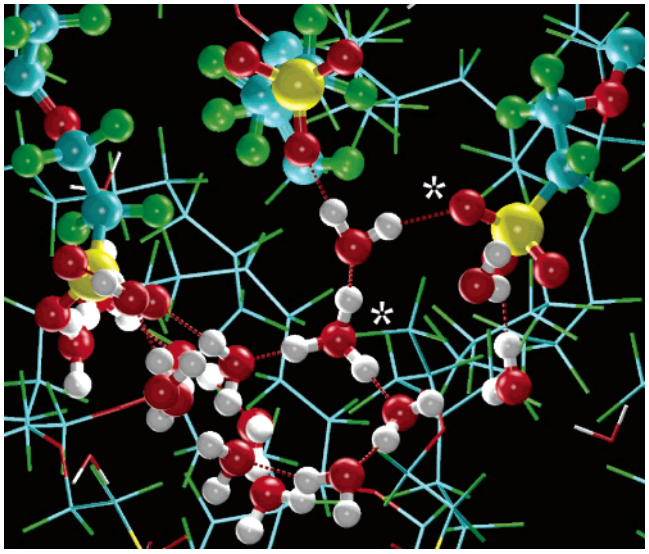

Figure 2. Representative configuration from the simulation depicting a solvent-separated ion pair (SSIP) configuration. Foreground atoms, oxygen (red), hydrogen (white), sulfur (yellow), carbon (cyan), and fluorine (green), are depicted in a ball-and-stick representation, while background atoms are depicted in a line representation. The marked hydronium oxygen and sulfonate oxygen are in a SSIP configuration.[46,47]

As any proton-transfer event must presumably involve the transient formation of Zundel and Eigen-like solvation structures, a more complete understanding of the proton-transfer process can be achieved by inspecting the relative distribution of these configurations along the "reaction coordinate",

$$q_{\mathrm{react}} = (c_1^{\,2} - c_2^{\,2}) \tag{3}$$

defined as the difference of the two largest EVB populations.[30,32] Figure 3 illustrates the free energy of the q_{react} coordinate from the SCI-MS-EVB Nafion simulation. For the symmetric Zundel configuration, the value of the coordinate is zero but otherwise takes finite values for increasingly Eigen-like configurations. As can be seen from Figure 3, on average, Eigen-like configurations are ~1 kcal/mol more stable than the symmetric Zundel configuration.

The relation between cation transfer among the CIP and SSIP regions and Grotthuss shuttling can be characterized through a combination of the interionic PMF and the corresponding q_{react} values. Free-energy surfaces were constructed by expanding the PMF curves of Figure 1 along the free-energy curve of the orthogonal q_{react} coordinate of Figure 3. Depicted in Figures 4 and 5 is this expansion for the CEC and hydronium cation descriptions, respectively.

It is apparent from the hydronium free-energy surface (Figure 5) that the Zundel-like configurations are favored when the water molecule bearing the bulk of the EVB amplitude (the hydro-

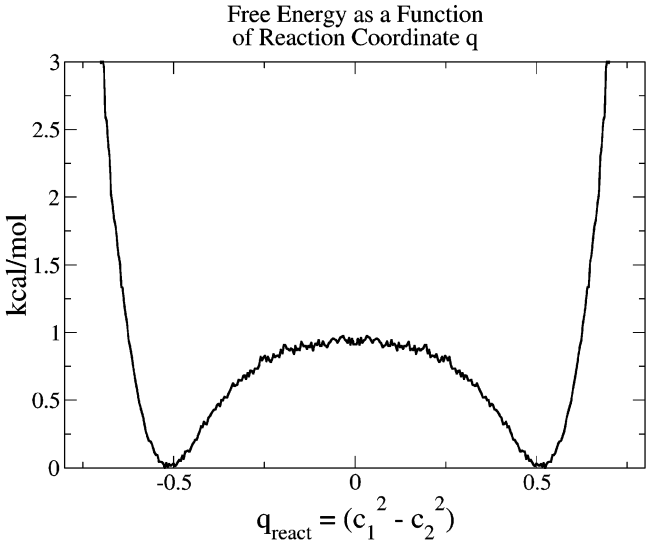

Figure 3. Free energy as a function of the difference between the two largest MS-EVB state populations.

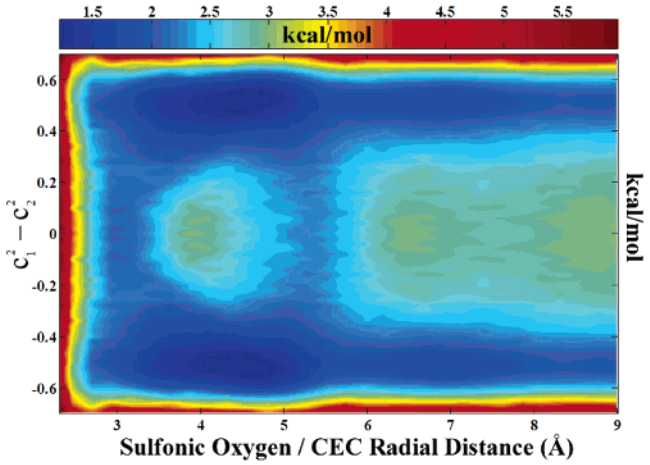

Figure 4. Free energy as a function of the difference between the two largest state populations and the radial distance between the sulfonate oxygen and the protonic CEC.

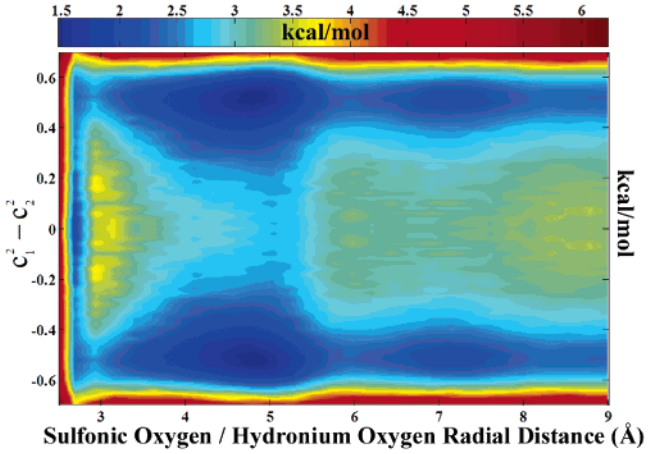

Figure 5. Free energy as a function of the difference between the two largest state populations and the radial distance between the sulfonate oxygen and hydronium oxygen.

nium) is in the CIP position. However, the transition between the CIP and SSIP regions along q_{react} is significantly higher in free energy for these Zundel-like configurations. The cation cannot readily transition these two regions in a Zundel-like structure and instead localizes into an Eigen-like configuration. The CIP/SSIP PMF barrier in the hydronium description is in essence the barrier for localizing the excess charge onto a single water molecule and repositioning this *same* molecule between the CIP and SSIP region.

By contrast, the free-energy surface for the CEC description in Figure 4 shows no minima in the CIP region for any value of q_{react}. When the CEC is directly adjacent to the sulfonate anion, Eigen-like configurations are stabilized; the bulk of the EVB population residing on that water in the CIP position, while a solvating water molecule of a potential Zundel moiety occupies the SSIP position. As the CEC moves away from the sulfonate anion, Zundel-like configurations become increasingly more accessible, resulting in a broad plateau of about 3 Å and $q_{react} \approx 0$. Configurations where the CEC is shifted away from the sulfonate anion (and hydronium oxygen) along the O−H−O bond of the cation are responsible for this plateau, as well as the minima about ∼2.75 Å and $q_{react} \approx 0$ on the hydronium surface. As the hydronium transitions laterally along q_{react} (away from values about $q_{react} \approx 0$), the CEC shifts back along the O−H−O bond and is again found directly adjacent to the sulfonate anion localized in Eigen-like configurations. Adjacent to the sulfonate anion, the hydronium cation is stabilized through Zundel-like configurations, with the CIP positioned water of the Zundel moiety trapped in a ∼0.7 kcal/mol minima. The CEC passes smoothly and barrierlessly along the O−H−O bond of the Zundel cation while the excess proton, and likewise, the identity of the hydronium, are transferred between the CIP and SSIP positions through the Grotthuss shuttling mechanism.

Interestingly, neither the CEC nor the hydronium descriptions are adequate to fully characterize the ion pair dissociation. The hydronium description could be incorrectly interpreted to show that the cation localizes on the CIP or SSIP water and transitions via this water displacement. Likewise, the CEC description fails to identify the significant barrier to solvent rearrangement, which essentially ensures that proton transfer between the CIP and SSIP positions takes place through the more accessible Zundel configurations. While the CEC definition is a meaningful description of the cation, significant insight into the associated solvent dynamics can be found by inspecting the nature of the water molecules that bear the bulk of the proton defect.

3.2. Diffusion. The previous consideration of the hydronium−sulfonate PMF suggests that the mechanism of proton transport about the sulfonate anion is dominated by the Grotthuss mechanism. While talk of Grotthuss shuttling may evoke images of discrete proton "hops" by means of bond formation and cleavage, this is certainly a simplification. No single proton can be uniquely identified as the excess proton or any oxygen−hydrogen pair unambiguously recognized as bonded; the diffusion of the CEC is continuous and smooth. Nevertheless, at long times, the diffusion of that state with the largest population is ostensibly equal to that of the CEC diffusion.

Within this approximation, the total displacement of the cation can be decomposed into two distinct contributions: one from the vehicular (or continuous) component due to the random molecular motions wherein the identity of the most protonated molecule remains constant, and the other due to the discontinuous identity change of the valence bond state with the largest population. If the displacement vector of the state with the largest amplitude (CEC_1) is written as a sum of this continuous and discrete displacement,

$$\vec{r}_{CEC_1}(t) - \vec{r}_{CEC_1}(0) = \Delta\vec{r}_{CEC_1} = \Delta\vec{r}_c + \Delta\vec{r}_d \qquad (4)$$

then the mean-squared displacement (MSD) can be written as

$$\langle \Delta\vec{r}_{CEC_1} \cdot \Delta\vec{r}_{CEC_1} \rangle = \langle \Delta\vec{r}_c \cdot \Delta\vec{r}_c \rangle + \langle \Delta\vec{r}_d \cdot \Delta\vec{r}_d \rangle + 2\langle \Delta\vec{r}_c \cdot \Delta\vec{r}_d \rangle \quad (5)$$

The *x* component of a representative trajectory (total, discrete, and continuous) is depicted in Figure 6. From the inset of Figure 6, the stepwise nature of the discrete portion of the total displacement is more clearly seen. While the continuous portion develops with small consistent displacements, the discrete portion proceeds with significant closely spaced multiple displacements punctuated by intervals of no change, which is symptomatic of relatively long-lived states. Most noteworthy is the near mirroring of the *x* component of the two displacement vectors, that is to say, the very nearly equal but opposite relative displacement of the two contributions. Although the displacement vectors of each component need not project onto any given axis in this manner, this particular trajectory developed along the *x*-axis in such a manner as to illustrate the interesting and strong anticorrelation between these two components of the total displacement.

The anticorrelation between the discrete and continuous displacement components is quantified through the MSD plots presented in Figure 7. Not only is the total diffusion less than the sum of its components, the diffusion of either component is remarkably greater than the total. The strong negative overlap (the last term of eq 5) of these two displacement vectors therefore results in a total diffusion less than that of either component. By contrast, discrete diffusion accounts for ~70% of the total MS-EVB2 hydronium diffusion (Figure 8) in bulk water with negligible negative correlation of the vehicular and discrete components.

3.3. Ion Pair Correlated Diffusion. It has been previously demonstrated through computer simulation that the diffusion of the protonic defect may be influenced by the motion of the sulfonate anions.[28] We have likewise observed here significant correlated motion of the ion pair and have quantified the time scale of these correlated motions through the distinct portion of the van Hove correlation function, given by[34]

$$G_d^{\alpha\beta}(r, t) = \frac{N_\alpha + N_\beta}{N_\alpha N_\beta} \langle \sum_{i=1}^{N_\alpha} \sum_{j=1}^{N_\beta} \delta(r - |r_i(0) - r_j(t)|) \rangle = \rho g_{\alpha\beta}(r, t) \quad (6)$$

Figure 9 depicts this correlation function (normalized by the average density) such that the sulfonate anions are chosen as the space and time origins.

At approximately 425 ps, the function develops a peak that is two to three times the average hydronium density. So, given that a sulfonate anion occupied a given position 425 ps earlier, the likelihood of finding a hydronium cation in this same position is nearly three times greater than that of the uniform hydronium density. This demonstrates a significant correlation in the local ion pair diffusion with a characteristic period of approximately 425 ps. It should be noted that, for long times comparable to the length of the trajectory and short radial distances, the data points become relatively sparse. For example, the 3.3 ps−0.5 Å bin about 425 ps and a radial distance of 0.75 Å has a value of 2.3 ± 0.2. Longer times and shorter distances are progressively statistically less reliable.

Given the observed strong correlated motion, it is easy to understand the apparent increase in diffusion seen by Spohr et al.[28] upon the transition from a tethered to a flexible model for the side chain. However, given the long characteristic period relative to the total simulation time and the comparatively low diffusion of both the pendant chain and the associated hydronium ion, it seems inappropriate to generalize this increase in local diffusion to an increase in macroscopic proton transport.

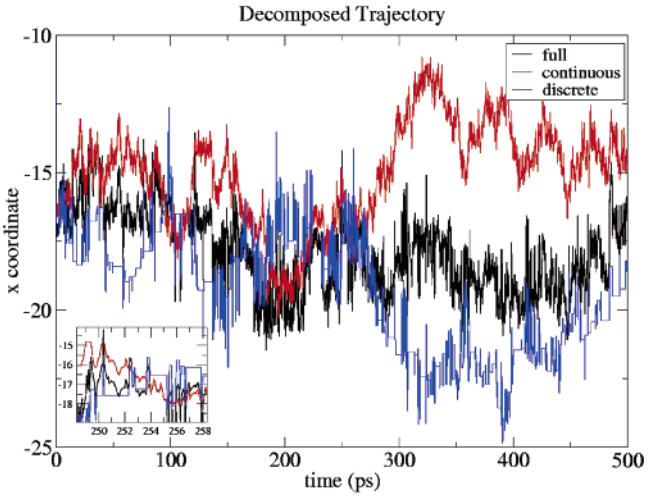

Figure 6. *x*-Coordinate of a representative trajectory for the CEC; the total trajectory (black), the continuous (vehicular, red), and discrete (Grotthuss, blue) components. The inset more clearly displays the stepwise nature of the discrete portion and the continuous nature of the vehicular portion.

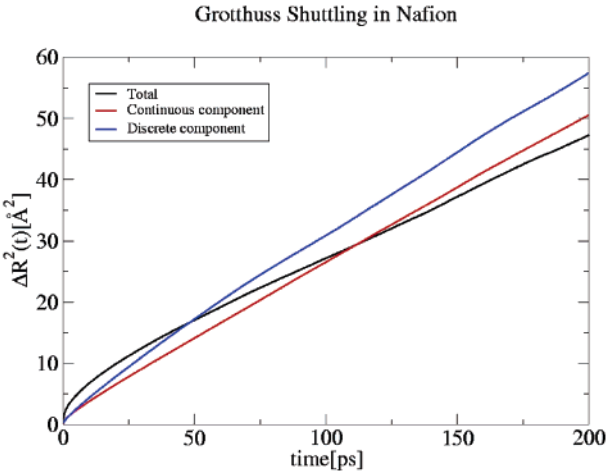

Figure 7. Total mean-squared displacement (black) and the continuous (red) and discrete (blue) components of the mean-squared displacement in Nafion.

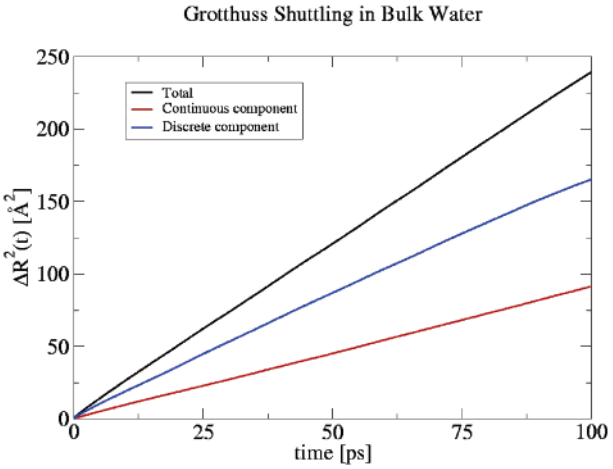

Figure 8. Total mean-squared displacement (black) and the continuous (red) and discrete (blue) components of the mean-squared displacement in bulk water

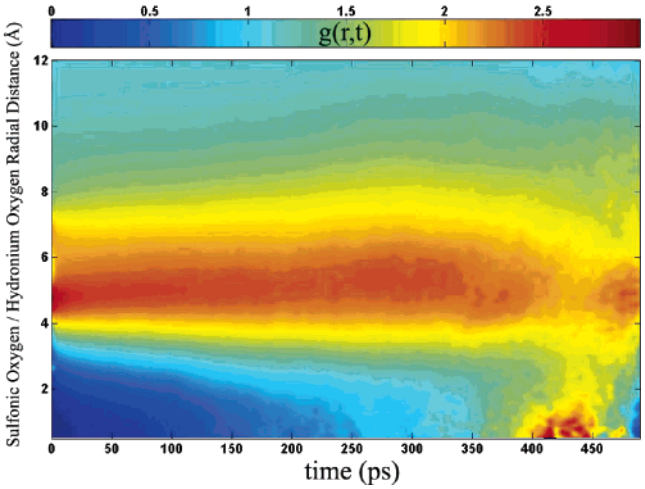

Figure 9. Distinct portion of the van Hove space−time correlation function eq 6 for the hydronium−sulfonate ion pair given the sulfonate anion as the space−time origin.

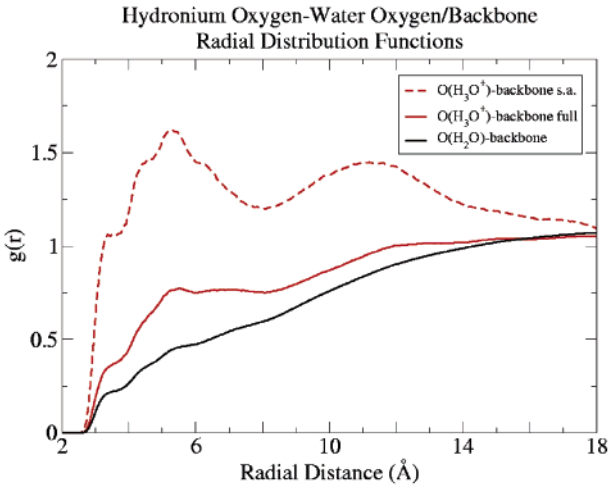

Figure 10. Radial distribution functions for the water oxygen−polymer backbone (black) and hydronium oxygen−polymer backbone (red). The restricted radial distribution function for the hydronium oxygen−polymer backbone (red dashed) is restricted to a π steradian solid angle with an apex formed from the vector extending from the hydronium hydrogen center-of-mass through the hydronium oxygen (the lone pair region).

It may very well be that the perceived increase in diffusion is simply an artifact of the correlated motion of the ion pair; that is, the more labile sulfonate ion of the flexible chain simply drags the hydronium cation as it diffuses about some mean position. However, because the pendant chain is ultimately bound to the comparatively static polymer backbone, the motion of this putative mean position may be inaccessible to the available molecular dynamics time scales.

3.4. Amphiphilic Association of the Hydronium Cation and the Hydrophobic Domain. It has recently been demonstrated that the amphiphilic-like character of the hydrated proton observed near the water liquid−vapor interface[35] and water clusters[36−38] extends to other mixed dielectrics such as methanol−water solutions.[39] Although the degree of amphiphilic association may be somewhat potential dependent,[40,41] there is compelling experimental support [42−45] for the surface enhancement observed in both empirical force field[35,38] and ab initio simulations.[36,37]

Radial distributions were therefore calculated between the hydronium cation and the hydrophobic polymer backbone (including all carbon and fluorine atoms but *excluding* those of the pendant chain) as well as between water and the hydrophobic backbone. It has been previously demonstrated that the anisotropic solvation of the hydronium cation results in a preferential hydrophobic association in the lone pair region of the ion's solvation shells.[39] With this in mind, the radial distribution restricted to a π steradian solid angle with an apex formed from the vector extending from the hydronium hydrogen center-of-mass through the hydronium oxygen (the lone pair region) was also calculated. These radial distribution functions are presented in Figure 10.

Although the solvation structures are very similar for the full water−backbone and hydronium−backbone distributions, the hydronium distribution displays larger populations at shorter distances. By itself, this is not definitive evidence for the preferential association of the hydronium lone pair region with the hydrophobic backbone and is possibly a consequence of the hydronium−sulfonate attraction and the proximity of the sulfonate pendant and the polymer backbone. However, the restricted radial distribution shows a significant lone pair region enhancement of the backbone population over the full distribution. Similar to that which has been previously demonstrated for the hydrophobic methyl groups of methanol,[39] there is a significant preferential anisotropic association of the hydronium with the hydrophobic polymer backbone.

4. Conclusions

The proton transport process about the sulfonate CIP/SSIP region was found in this work to proceed largely through the Grotthuss shuttling mechanism. A decomposition of the hydronium MSD shows that the overall diffusion process is a highly correlated exchange between diffusion through vehicular diffusion of the transient dominant state and the fluctuating bond topology, resulting in a relatively small net diffusion. Furthermore, the distinct portion of the van Hove correlation function shows the ion pair diffusion is correlated with a characteristic time scale of several hundred picoseconds.

In total, our results indicate that the sulfonate ion significantly influences the diffusion of the protonic defects in a hydrophilic pocket of Nafion. As the transiently dominant hydronium state diffuses away from the sulfonate ion, the fluctuating bond topology "resets" the position of the dominant state back to some mean position relative to the adjacent sulfonate ion. The sulfonate ions effectively act as proton "traps", limiting the hydronium diffusion primarily to the long time correlated ion pair motions. This may in part explain why side chain length variants of Nafion-like polymers, such as the Dow membrane or Aciplex, exhibit varying transport rates. A shorter pendant chain may restrain the sulfonate groups from deeply penetrating the hydrophobic phase and trapping the excess protons in the bulk water region where transport could be the greatest. On the other hand, perhaps the shorter pendant chains allow the hydrated proton to more closely interact with the hydrophobic portion of the polymer, for which it has a demonstrated affinity, enabling transport along the hydrophilic/hydrophobic boundary. These possibilities will be more closely explored in future research.

Acknowledgment. This research was supported by the Department of Energy Basic Energy Sciences program (grant no. DE-FG02-05ER15724) and the U.S. Army Research Laboratory and the U.S. Army Research Office (grant no. DAAD 19-03-1-0121). We thank Dr. Kim Wong and Mark Maupin for their critical reading of the manuscript.

References and Notes

(1) Alberti, G.; Casciola, M.; Massinelli, L.; Bauer, B. *J. Membr. Sci.* **2001**, *185*, 73.
(2) Li, Q.; He, R.; Jensen, J. O.; Bjerrum, N. J. *Chem. Mater.* **2003**, *15*, 4896.
(3) Heinzel, A.; Barragán, V. M. *J. Power Sources* **1999**, *84*, 70.
(4) Wu, H.; Wang, Y.; Wang, S. *J. New Mater. Electrochem. Syst.s* **2002**, *5*, 251.
(5) Uitto, O. D.; White, H. S.; Aoki, K. *Anal. Chem.* **2002**, *74*, 4577.
(6) Kreuer, K. D. *J. Membr. Sci.* **2001**, *185*, 29.
(7) Laporta, M.; Pegoraro, M.; Zanderighi, L. *Phys. Chem. Chem. Phys.* **1999**, *1*, 4619.
(8) Loppinet, B.; Gabel, G.; Williams, C. E. *J. Phys. Chem. B* **1997**, *101*, 1884.
(9) Paddison, S. J.; Paul, R.; Zawodzinski, T. A. *J. Chem. Phys.* **2001**, *115*, 7753.
(10) Eikerling, M.; Kornyshev, A. A.; Kuznetsov, A. M.; Ulstrup, J.; Walbran, S. *J. Phys. Chem. B* **2001**, *104*, 3646.
(11) Paddison, S. J. *J. New Mater. Electrochem. Syst.* **2001**, *4*, 197.
(12) Li, T.; Wlaschin, A.; Balbuena, P. B. *Ind. Eng. Chem. Res.* **2001**, *40*, 4789.
(13) Eikerling, M.; Paddison, S. J.; Pratt, L. R.; Zawodzinski, T. A. *Chem. Phys. Lett.* **2003**, *368*, 108.
(14) Paddison, S. J.; Pratt, L. R.; Zawodzinski, T. A.; Reago, D. W. *Fluid Phase Equilib.* **1998**, *150*, 235.
(15) Paddison, S. J.; Eikerling, M.; Zawodzinski, T. A.; Pratt, L. R. Molecular Modeling of Proton Conduction in Polymer Electrolyte Membranes of Nafion Type. In *Proceedings of the ICCN 2002 International Conference on Computational Nanoscience, San Juan, Puerto Rico, April 22−25, 2002;* The Applied Computational Research Society: Cambridge, MA, 2002.
(16) Vishnyakov, A.; Neimark, A. V. *J. Phys. Chem. B* **2001**, *105*, 7830.
(17) Vishnyakov, A.; Neimark, A. V. *J. Phys. Chem. B* **2001**, *105*, 9586.
(18) Rivin, D.; Meermeier, G.; Schneider, N. S.; Vishnyakov, A.; Neimark, A. V. *J. Phys. Chem. B* **2004**, *108*, 8900.
(19) Jang, S. S.; Molinero, V.; Cagin, T.; Goddard, W. A. I. *J. Phys. Chem. B* **2004**, *108*, 3149.
(20) Elliot, J. A.; Hanna, S.; Elliot, A. M. S.; Cooley, G. E. *Phys. Chem. Chem. Phys.* **1999**, *1*, 4855.
(21) Petersen, M. K.; Wang, F.; Blake, N. P.; Metiu, H.; Voth, G. A. *J. Phys. Chem. B* **2005**, *109*, 3727.
(22) Gierke, T. D.; Munn, G. E.; Wilson, F. C. *J. Polym. Sci.* **1981**, *19*, 1687.
(23) Hsu, W. J.; Barkely, J. R.; Meakin, P. *Macromolecules* **1980**, *13*, 198.
(24) Grotthuss, C. J. T. (d) *Ann. Chim. (Paris)* **1806**, *58*, 54.
(25) Agmon, N. *Chem. Phys. Lett.* **1995**, *244*, 456.
(26) Tuckerman, M.; Laasonen, K.; Sprik, M.; Parrinello, M. *J. Chem. Phys.* **1995**, *103*, 150.
(27) Lapid, H.; Agmon, N.; Petersen, M. K.; Voth, G. A. *J. Chem. Phys.* **2004**, *122*, 014506.
(28) Spohr, E.; Commer, P.; Kornyshev, A. A. *J. Phys. Chem. B* **2002**, *106*, 10560.
(29) Seeliger, D.; Hartnig, C.; Spohr, E. *Electrochim. Acta* **2005**, *50*, 4234.
(30) Day, T. J. F.; Soudackov, A. V.; Cuma, M.; Schmitt, U. W.; Voth, G. A. *J. Chem. Phys.* **2002**, *117*, 5839.
(31) Wang, F.; Voth, G. A. *J. Chem. Phys.* **2005**, *112*, 144105.
(32) Schmitt, U. W.; Voth, G. A. *J. Chem. Phys.* **1999**, *111*, 9361.
(33) Voth, G. A. *Acc. Chem. Res.* **2006**, *39*, 143.
(34) Hove, L. V. *Phys. Rev.* **1954**, *95*, 249.
(35) Petersen, M. K.; Iyengar, S. S.; Day, T. J. F.; Voth, G. A. *J. Phys. Chem. B* **2004**, *108*, 14804.
(36) Iyengar, S. S.; Day, T. J. F.; Voth, G. A. *Int. J. Mass Spectrom.* **2005**, *241*, 197.
(37) Iyengar, S. S.; Petersen, M. K.; Day, T. J. F.; Burnham, C. J.; Tiege, V. E.; Voth, G. A. *J. Chem. Phys.* **2005**, *123*, 084309.
(38) Burnham, C. J.; Petersen, M. K.; Day, T. J. F.; Iyengar, S. S.; Voth, G. A. *J. Chem. Phys.* **2006**, *124*, 024327.
(39) Petersen, M. K.; Voth, G. A. *J. Phys. Chem. B* **2006**, *110*, 7085.
(40) Mucha, M.; Frigato, T.; Levering, L. M.; Allen, H. C.; Tobias, D. J.; Dang, L. X.; Jungwirth, P. *J. Phys. Chem. B* **2005**, *109*, 7617.
(41) Dang, L. X. *J. Chem. Phys.* **2003**, *119*, 6351.
(42) Shultz, M. J.; Schnitzer, C.; Simonelli, D.; Baldelli, S. *Int. Rev. Phys. Chem.* **2000**, *19*, 123.
(43) Miranda, P. B.; Shen, Y. R. *J. Phys. Chem. B* **1999**, *103*, 3292.
(44) Radüge, C.; Pflumio, V.; Shen, Y. R. *Chem. Phys. Lett.* **1997**, *274*, 140.
(45) Petersen, P. B.; Saykally, R. J. *J. Phys. Chem. B* **2005**, *109*, 7976.
(46) Illustration rendered with Raster3D. Merritt, E. A.; Bacon, D. J. *Methods Enzymol.* **1997**, *277*, 505.
(47) Illustrations created with the visualization package VMD. Humphrey, W.; Dalke, A.; Schulten, K. *J. Mol. Graphics* **1996**, *14*, 33.